JSST
VOL.15 / ISSUE 1-1 / SPRING SPECIAL 2022/
Print ISSN: 2008-4560/Online ISSN: 2324-4516
DOI:10.30699/JSST.2022.1169
Pages: 35-44 / Researcher Paper / Submit: 2019.02.25 / Accepted: 2019.10.23 /Publish Online: 2022.04.04

Strap-On Boosters Separation Analysis using Coupled Simulation of Constraint Dynamics and Time-Dependent CFD

Mostafa Jafari [1] and Alireza Toloei [2]*

1, 2. Faculty of New Technologies and Aerospace Engineering, Shahid Beheshti University, Tehran, Iran

* **toloei@sbu.ac.ir**

A numerical dynamic-aerodynamic interface for simulating the separation dynamics of constrained strap-on boosters jettisoned in the atmosphere is presented in this paper. Two commercial solvers: a 6DOF multi-body dynamic solver and a numerical time-dependent flow solver are integrated together with an interface code to constitute a package that presents real-time dynamic/aerodynamic coupled analysis. Dynamic unstructured mesh approach is employed using local remeshing methods in respect of bodies' motion with a second-order upwind accurate 3D Euler solver. This interface can simulate the interaction of multi body separation dynamics with aerodynamic effects to complete separation mechanisms like springs, thrusters, joints, and so on. The flow solver is validated by the Titan IV launch vehicle experimental data. The separation integration is used for a typical launch vehicle with two strap-on boosters using spring ejector mechanism and spherical constraint joints acting in the dense atmosphere. Hence, the aim of the presented interface is to facilitate the integration of complicated separation mechanisms with a full numerical CFD aerodynamic solver.

Keyword: Strap-On Boosters, Separation Analysis, 6DOF multi body dynamic, Numerical time dependent flow solver, Spring ejector mechanism, CFD, Dynamic mesh

Calculator

K	spring stiffness
C	viscous damping ratio
R	spring displacement
L_0	spring initial length
F_{max}	spring initial length

Introduction

Strap-on boosters are used to increase the payload capabilities of launch vehicles. Adding Boosters to the vehicle core makes the design and manufacture of launcher more complex. One of the important issues in the design and construction of these launchers is the safe booster separation from the core vehicle. Any unexpected instability in this section or any catastrophic collision and in general, any factor that prevents successful separation, can tend the entire mission to fail. Since the booster separation usually takes place in the dense atmosphere, in addition to the dynamic effect of ejection mechanisms, aerodynamic flow around the launch vehicle is also important [1]. Many researchers have investigated this field for several years. Meakin and Suhs of NASA Ames analyzed the solid booster (SRB) separation of a space shuttle with a Navier–Stokes solver, using a prescribed trajectory for dynamic analysis of body motion [2]. Lochan and Adimurthy analyzed the separation dynamics of strap-on boosters. They used wind tunnel data for the measurement of aerodynamic forces [3, 21, 22]. Lijewski and Suhs developed an unsteady technique for store separation from a delta wing [4]. In addition, Taylor et al. for the Titan IV with two boosters and Azevedo and Moraes for the AVLS launch vehicle with four boosters carried out similar analysis using steady-state aerodynamics without considering the relative motion of boosters [5, 6]. Kim et al. were among the first researchers that used numerical dynamic-aerodynamic coupling to simulate strap-on boosters' separation [8]. They also had studied the effects of flow turbulence in

1. PhD Student

2. Associate Professor (Corresponding Author)

booster separation [9]. In both recent cases, in accordance with conventional methods, dynamic mesh method (in aerodynamics) and the integrated dynamic code were used briefly and simply without any complex separation mechanisms for solving separation problems. In fact, the simulation was based on the aerodynamic analysis with an integrated simple 6DOF dynamic code. In other cases, separation mechanisms have to be prescribed in the calculations [9, 10, and 11]. Commercial flow solvers have been of great interest in separation analysis. FLUENT and OVERFLOW can be considered as good paragon of these solvers that have been frequently mentioned in the literature [9, 12, 13]. Both of these solvers utilize a 6DOF rigid body motion code with simple and prescribed separation mechanism, integrated into the unsteady Navier–Stokes (Euler) solver using an automated grid adaption method.

In the early 2000s, separation process was considered as one of the key technologies to develop the next generation of orbiter with reusability [12]. For this purpose, such software, like ConSep and Sepsim using ADAMS (Automatic Dynamic Analysis of Mechanical Systems) solver aided by wind tunnel results have been developed [13, 14, and 15]. In such software, complex full separation mechanisms can be modeled; but large aerodynamic coefficient databases are needed for calculation of aerodynamic effects on booster separation. In 2006, Pamadi et al. had examined the shuttle booster separation using Concep software and wind tunnel results at NASA [12]. In addition, this work had been done by the CFE/POST2 software [16]. In this software, notwithstanding the powerful dynamic analysis, aerodynamic modeling is incomplete and for example, unsteady effects of flow and boosters velocity effects are missed in analysis. Moreover, the aerodynamic databases are multidimensional and too large [12, 21, 22], and therefore, not suitable for developing new vehicle design. Based on what has been stated, the previous studies just focused on one of the dynamic or aerodynamic analysis using a brief form of the other (analysis) for completing their results. So, the separation analysis of strap-on boosters in atmosphere with consideration of complicated mechanisms (such as constrained dynamics) and unsteady aerodynamic effects was not mentioned in the open literature.

This paper (in continuation of previous article by the authors [1]) is focused on developing a dynamic/aerodynamic coupled solver to simulate the separation of strap-on boosters' using constraint dynamics and time-dependent CFD. Therefore, two commercial solvers, MSC Adams and Ansys/Fluent are integrated together with an innovative Matlab/Simulink interface to constitute a powerful package that presents real-time dynamic/ aerodynamic coupled analysis. Independency of dynamic and aerodynamic solvers allows modeling of any complex separation dynamic mechanisms, while the unsteady flow analysis is implemented. Consequently, this method can simulate several multi-physic problems such as booster separation with more accuracy than conventional methods. For example, modeling of real-time joint separation in the presence of unsteady aerodynamics is proven. Also, the interface was validated by simulating a transonic store separation event compared with experimental data by the authors [19, 20].

Problem Description

The 6DOF dynamics of separation of strap-on boosters from the fixed core using spring ejector mechanism and spherical joints is simulated. External geometry of the launch vehicle with springs and joints positions can be seen in Fig.1.

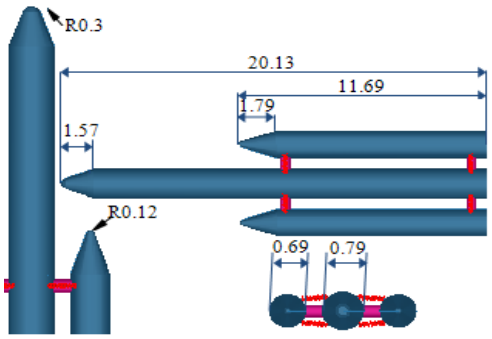

Fig .1: launch vehicle configuration (meter)

Launch Vehicle Aerodynamics with Strap-on Boosters

In order to calculate the aerodynamic forces and moments, a numerical solution of unsteady flow with an implicit upwind accurate 3D Euler solver is used. A dynamic unstructured tetrahedral mesh adoption approach using a combination of spring-based smoothing [4] and local remeshing [5] is automatically employed in respect of bodies' motion and determining the location of new nodes. In this analysis, the entire field is divided into a total of about 900000 tetrahedral cells. A view of gridded domain can be seen in Fig. 2. Separation is done at an altitude of 21 km with 4728.9 Kpa gage pressure at Mach 1.6, and the airflow around the launch vehicle is assumed as perfect gas. Pressure distribution in the flow field around the launch vehicle and strap-on boosters before the separation are shown in Fig. 3.

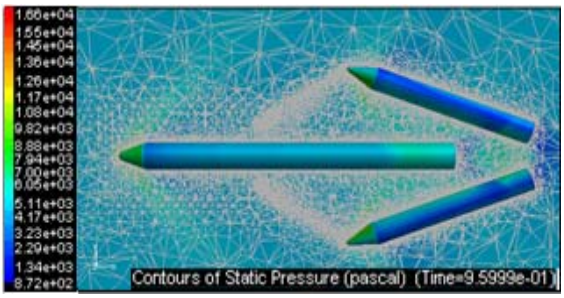

Fig. 2: A view of gridded domain (Dynamic Mesh Updating)

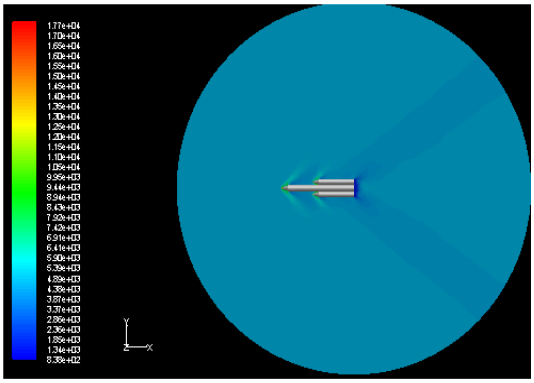

Fig. 3: flow field around the launch vehicle

Flow solver validation

To validate the flow solver, wind tunnel data of the Titan IV has been used (Fig. 4, 5). In this test, the free stream Mach number is 1.6, with zero angle of attack and 36000 meters of separation height. In Fig. 4, the calculated pressure contour for Titan VI cross-section shows that good agreement between the numerical solution and wind tunnel results can be observed in most regions. Slight differences in connecting points of the core vehicle and boosters are because of a connecting cable in the wind-tunnel test [1].

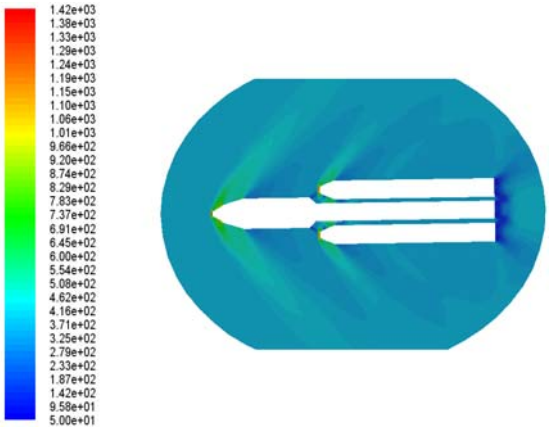

Fig. 4: Pressure contour around the Titan-IV launch vehicle

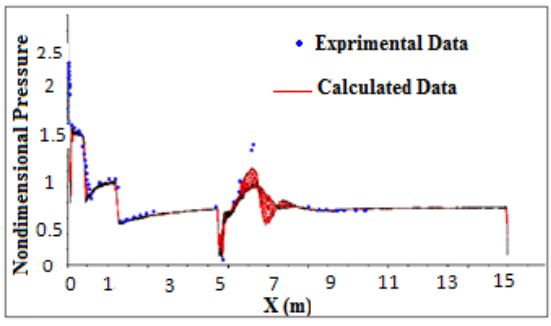

Fig. 5: Comparison of computed surface pressure with wind-tunnel data along the centerline

Mesh Independence

Pressure changes in the longitudinal direction of the main body of the launch vehicle (before separation) have been calculated for different mesh sizes. Three samples of these changes can be seen in Fig. 6. The calculated pressures are roughly similar in both normal and fine cases, so the normal mesh size of about 900000 cells has been selected.

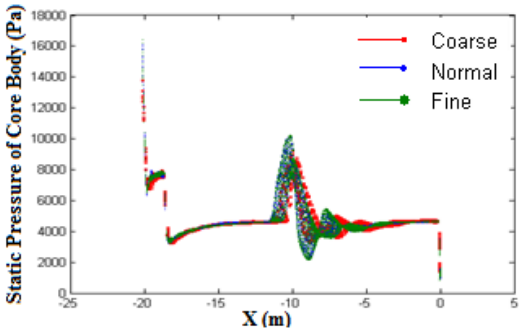

Fig. 6: Computed surface pressure along the centerline for different grid size

Boosters Separation Dynamics

The boosters' separation dynamics is derived using the constraint force equation (CFE) methodology. This method provides a framework to compute the internal forces and moments acting on two bodies with specified degrees of freedom and applies them as external forces and moments to each body. Then, the motion of each body can be simulated independently like multiple free bodies. Thus, CFE methodology provides the missing link to model the stage separation [17].

The equations of motion for each rigid body can be expressed with six scalar equations obtained from Newton's second law:

$$F_i + \sum_i F_{ij}^{(con)} = m_i \ddot{x}_i$$

$$T_i + \sum_i [(\rho_{ij} \times F_{ij}^{(con)}) + T_{ij}^{(con)}] = I_i.\dot{\omega}_i + \omega_i \times I_i.\omega_i$$

where the i subscripts represent the i^{th} vehicle, and the j subscripts represent the j^{th} local joint connection on the rigid body i. F_i and T_i represent the resultant external forces and torques, excluding constraint loads, m_i is the vehicle mass, $\ddot{x}_i$ is the linear acceleration of the mass center, I is the inertia dynamic with respect to the mass center of the vehicle i, ω_i is the absolute angular velocity, and $\dot{\omega}_i$ is the time rate of change of angular velocity. $\sum_i F_{ij}^{(con)}) + T_{ij}^{(con)}] = I_i.\dot{\omega}_i + \omega_i \times I_i.\omega_i$ $F_{ij}^{(con)}$ and $T_{ij}^{(con)}$ represent the resultant constraint force and torque vectors acting on the body i at its j^{th} joint location. The ρ_{ij} vector defines the j^{th} joint connection position relative to the center of mass of vehicle i. Details regarding the formulations are available in the literature [17,18].

Separation Mechanisms Model

Separation Springs

The equation used to calculate the spring force:

$$Fs = -C\left(\frac{db}{dt}\right) - K(r\text{-}L_0) + F_{max}$$

That

K= spring stiffness

C= viscous damping ratio

R= spring displacement

L_0= spring initial length

F_{max}= spring initial length

The characteristics of spring ejector mechanism can be seen in Fig. 555 and table 2, according to them, all of the springs are linear translational (stroke of 0.167 meters). These ejectors are separated from the launch vehicle at F_s= 450 N. Spring force, as a function of displacement is shown in Fig. 9:

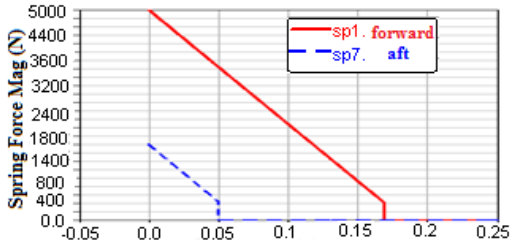

Fig.7: spring ejectors force, as a function of displacement

In Fig. 7, the upper curve with an initial force of 5000 N represents the force variation of forward ejectors (Number 1,2,5,6) and dashed curve with an initial force of 1800 Newton represents the force variation of aft ejectors (Number 3,4,7,8). These springs stroke, and the maximum and the minimum force of them are visible in this figure. This diagram as a function of time is shown in Fig. 8. According to Fig. 8, aftward springs (with maximum force of 1800 N) start working at approximately 0.15 second later than forward ones and after disconnection of related joints. In this simulation, the gravity is assumed 9.80665 m/s2 along the axis of the launch vehicle toward its end (+ x).

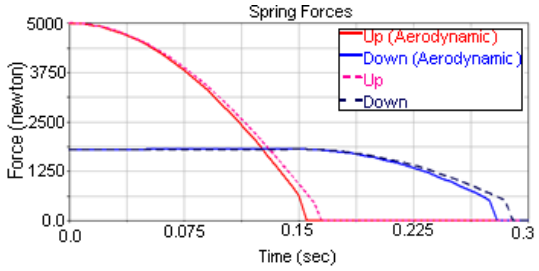

Fig. 8: Time Variation of spring ejectors force

Spherical Constraint Joints Modeling

In this simulation, spherical constraint joints have been used to connect the boosters on the launch vehicle. For all of constraints, ball and socket attachments have been assigned. One of these attachments is connected to the booster (ball) and the other is connected to the core vehicle. The translational motion of spherical constraints has been limited in three dimensions, wherein there is no interference with the rotational motion. If A is pointed to the joint on the core and B pointed to the same location on the booster, one can obtain:

$$\begin{Bmatrix} D_x(A,B) = 0 \\ D_y(A,B) = 0 \\ D_z(A,B) = 0 \end{Bmatrix} * C_{sep}$$

So, the zero function (C_{sep}):

$$C_{sep} = \begin{cases} 1 & \text{time} \le 0.001 \text{ sec} \\ 0 & \text{time} \ge 0.001 \text{ sec} \end{cases}$$

As a result of the above equation, forward constraints separate from launch vehicle, after 0.001 sec. The angle condition has been used to disconnect the two aftward attachments. When the relative angle between booster and vehicle body reaches to 1deg, the joints disconnect.

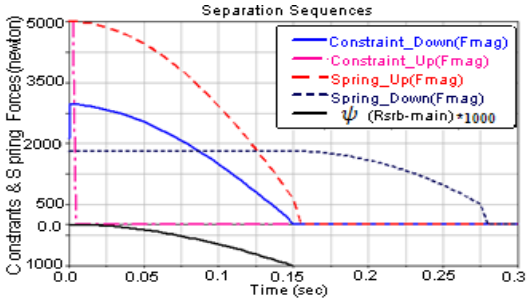

Fig. 9: Separation sequence of spring ejectors and joints

$$C_{sep2} = \begin{cases} 1 & (\psi_{booster} - \psi_{main}) \le 1 \text{ deg} \\ 0 & (\psi_{booster} - \psi_{main}) \ge 1 \text{ deg} \end{cases}$$

In Fig. 9, the joints separation sequence and the sample forward and aftward springs are shown. The constraint (number) 3 is similar to the constraint 1, and the constraint 4 is similar to the constraint 2. As could be seen in Fig. 9, two upper constraints have been disconnected at the start of simulation (t=0.001 sec). The disconnection of two lower constraints has occurred when the relative angle between them reached to 10 deg (as shown in the lower segment of Fig. 9). It is noticeable that in the present plan, all of the constraints and springs have the same cross-sectional areas, so the corresponding spring of any constraints is not contributed to the solution until the separation of the constraint occurs. This fact results that, the operation of springs at the lower section, begins at t=0.09 sec. The block diagram of this solution could briefly be seen in the following graph (Fig.9). According to this algorithm, the code calculating the dynamic of the motion reports the position of vehicle to the flow solver, so the solver could derive the aerodynamic forces and moments in each time step. Then, this code calculates the linear and angular velocities of

the vehicle, using the results of forces and moments. Consequently, the mesh in the next step is corrected. In this algorithm, both the dynamic and the aerodynamic solvers are connected to the main interface as two independent external functions (Fig.9, Fig.10).

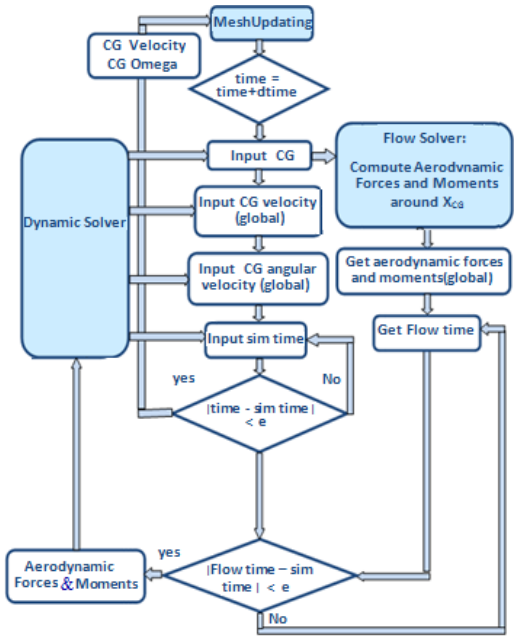

Fig. 10: The block diagram of Dynamic and Aerodynamic coupling

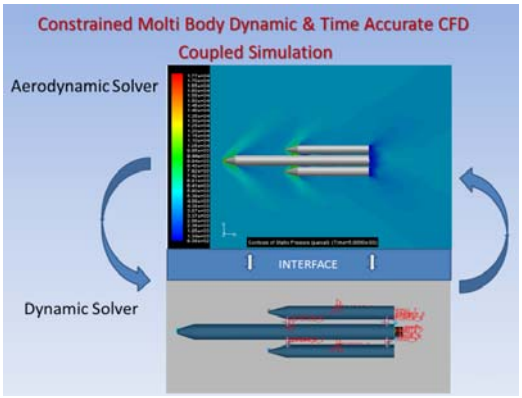

Fig. 11: Dynamic / Aerodynamic Solvers Interface

Results

The results are given for the first 1.1 seconds of the motion, with aerodynamic effects and without it. All the graphs are plotted for the left booster and the right booster while the core vehicle is fixed. Without aerodynamic effects, there is no displacement in the z-direction and the motion is in xy plane. Considering that joints are active for approximately 0.15 seconds and spring ejectors 0.3, so in the case of no aerodynamic, velocity in separation direction(y) remains constant after 0.3 seconds.

Parametric Study

This section examines the path diagrams and some of the parameters affecting them, such as aerodynamic effects of flow on booster separation and some parameters like boosters mass, strength of spring ejectors, booster separation angle (joints separation). For this purpose, the separation mechanism is determined for the sample launch vehicle that its size and geometry and also flow characteristics around it was explained in the previous section. Simulation inputs are as follows. We call this simulation as the standard mode and the effect of parameters variations will be analyzed regarding the standard mode.

Simulation Inputs (Standard Mode)

Mass properties of the launch vehicle and two strap-on boosters:

Table 1: mass properties of the launch vehicle and two strap-on boosters and characteristics of 8 used springs (springs 1, 2, 5, and 6 in forward section and springs 3, 4, 7, and 8 in aft section):

Launch Vehicle	Strap-on Booster
M : 22800.0 kg	M :2000.0 kg
IXX : 7000.0 kg-meter^2	IXX : 477.0 kg-meter2
IYY : 700000.0 kg-meter^2	IYY : 19077.0 kg-meter^2
IZZ : 700000.0 kg-meter^2	IZZ : 19077.0 kg-meter^2
IXY : 0.0 kg-meter^2	IXY : 0.0 kg-meter2
IZX : 0.0 kg-meter^2	IZX : 0.0 kg-meter2
IYZ : 0.0 kg-meter^2	IYZ : 0.0 kg-meter
Without initial speed	Without initial speed

Table 2: characteristics of spring separation mechanism

Spring ejectors	Number:1,2,5,6 (forward)	Number:3,4,7,8 (aft)
Type	Translational	Translational
Damping Coef.	0.0 N. S/ m	0.0 N-s/ m
Stiffness	27000.0 N. S	27000.0 N. S
Initial force (Fmax)	5000.0 N	1800.0 N
Final Force	450.0 N	450.0 N
Initial Length	0.9762 m	0.9762 m

In this case, the spherical joints in the forward section cutoff at 0.0001 seconds after separation. Therefore, the boosters begin to rotate about aft joints until the boosters reach the angle of 1 degree (about z-axis) and then aft joints separate from the core vehicle.

Comparison of Boosters Separation, with Different Mass

Separation simulation for boosters with 650 kg mass (approximately 30% of previous case) is also studied. With booster mass reduction, moment of inertia and angular velocities also increases. Due to the interaction of boosters' angle and velocity with aerodynamic effects, aerodynamic forces also increase, that can double the separation velocity. This can be seen in Fig. 12.

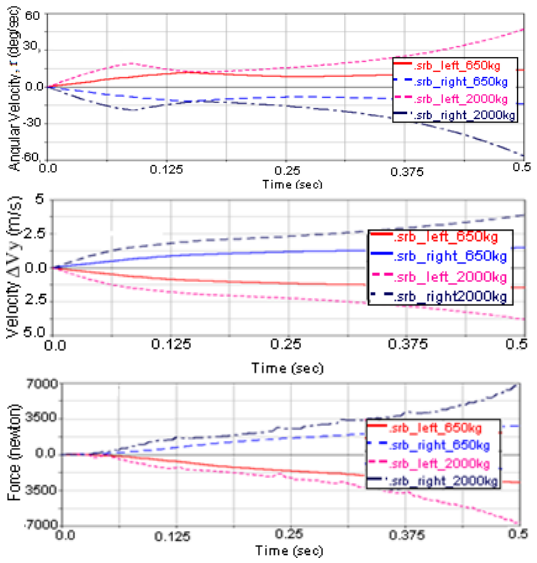

Fig.12: Time variations for 650 kg & 2000 kg boosters, A: Variation of the left & right boosters' relative velocities (Δy), B: Variation of the left & right boosters angular velocities (r), C: Variation of aerodynamic forces

Comparison of Boosters Separation, Using Spring Ejectors with Different Power

In addition to the standard case, which is referred to in tables 1 and 2, the simulation is also performed using spring ejector mechanisms with different power, and the results can be seen in Fig. 11, it means: $F_s = \alpha F_{standard2}$, α=0, 1, 1.5, 3

According to Fig. 13 that shows the location of the strap-on boosters at 1.1 seconds after separation, the desirable effect of the spring power increase can be seen. In this figure, the nearest booster to the core is resulted from the case without ejector spring. Other three modes: standard mode, 1.5 and 3 times greater than standard mode are also shown in Fig. 13. According to this figure, power of selected spring ejectors in standard mode (according to table 2) is appropriate and also the safe separation is achieved without increasing the power. Pressure contour variation around the launch vehicle and boosters during strap-on boosters' separation is shown in Fig. 15 for the four mentioned modes. Force variations for these four modes with respect to time are shown in Fig. 14.

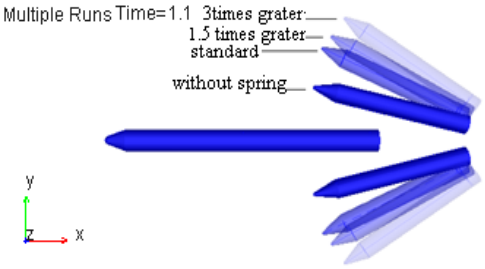

Fig. 13: Boosters' position at t=1.1sec after separation (using ejector springs with different power - with 1 degree of separation angle condition)

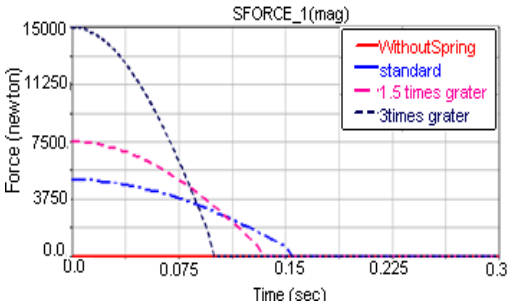

Fig. 14: Time variation of spring$_1$ force for spring ejectors with different powers

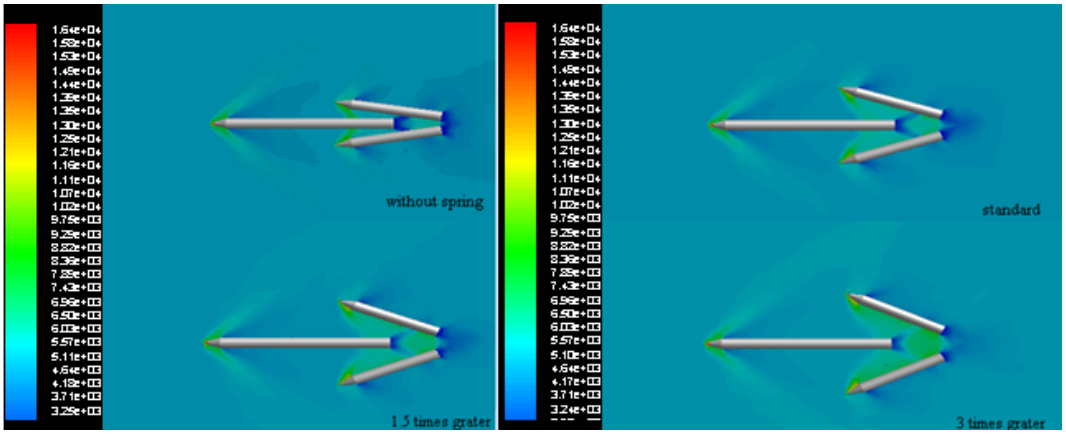

Fig. 15: Pressure contour variation around the launch vehicle and boosters at t=1.1sec after separation (using ejector springs with different powers - with 1 degree of separation angle condition

In figures 16 to 21, path diagrams of strap-on boosters for spring ejectors with different powers (with 1 degree of separation angle condition) are displayed. Results for the first 1.1 seconds of motion are given with presence of aerodynamic effects. In Fig. 16 and Fig. 17, variations of relative distances of boosters' center of mass with time (ΔX, ΔY, and ΔZ) and variations of relative velocities of center of mass with time (ΔVx, ΔVy, and

ΔVz) in presence of aerodynamic effects and for spring mechanisms with different powers can be seen. According to these figures, the desirable effect of ejector power increasing in improving separation performance is observed. This is also seen in other diagrams. In Fig. 18, which is related to the linear acceleration, the fracture points represent joints' disconnection and a complete booster separation from launch vehicle. Also, angular velocities, aerodynamic forces and moments of separated boosters can be seen in figures 19, 20, and 21.

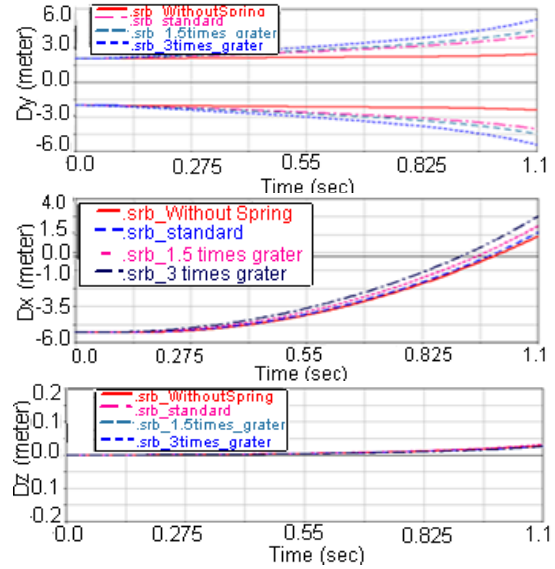

Fig. 16: Variation of strap-on boosters relative distances, ΔX, ΔY, and ΔZ (relative to the core CM) with time using spring ejectors with different powers (in the presence of aerodynamic effects)

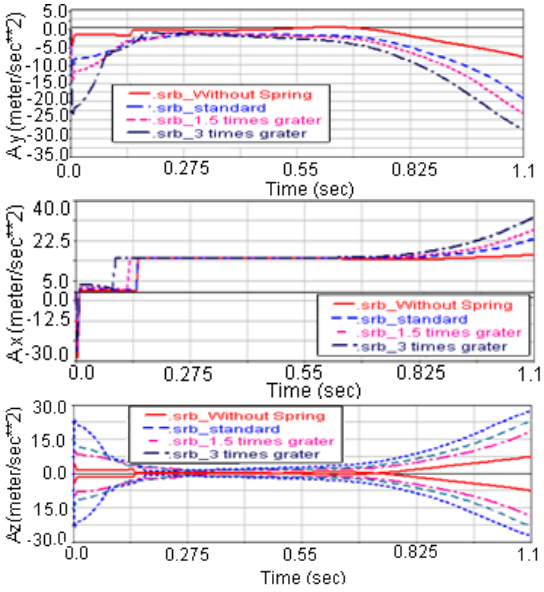

Fig. 18: Variation of the left & right boosters' relative translational accelerations, Ax, Ay, and Az (relative to the core CM) with time using spring ejectors with different powers (in the presence of aerodynamic effects)

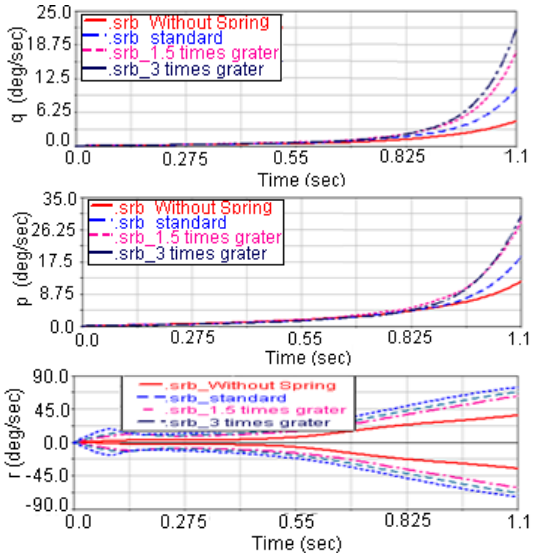

Fig. 19: Variation of the left & right boosters' angular velocities, p, q, and r, with time using spring ejectors with different powers (in the presence of aerodynamic effects)

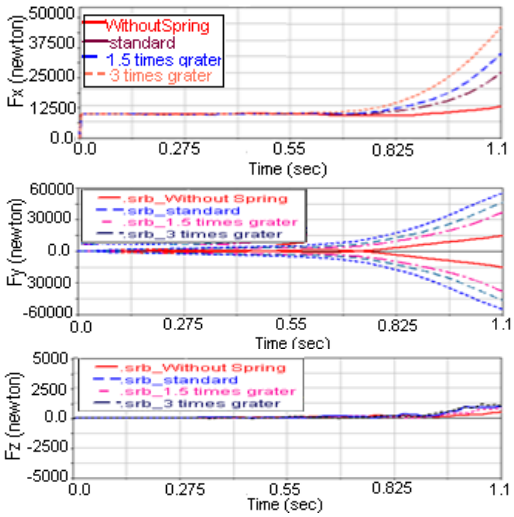

Fig. 20: Variation of aerodynamic forces with time on left and right boosters using spring ejectors with different powers (in the presence of aerodynamic effects)

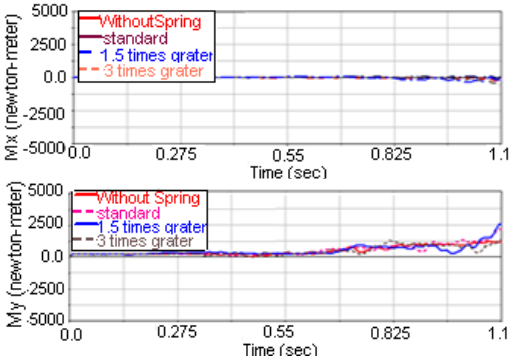

Fig. 21 Variation of aerodynamic moments with time on left and right boosters using spring ejectors with different powers

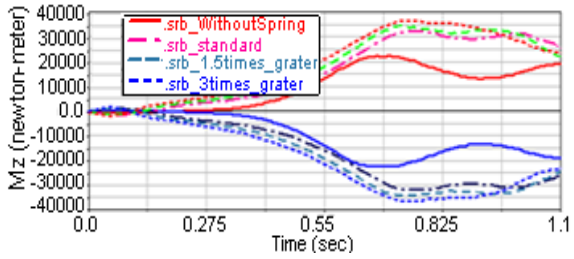

(Continuation) Fig. 21: Variation of aerodynamic moments with time on left and right boosters using spring ejectors with different powers (in the presence of aerodynamic effects)

Comparison of Boosters Separation with Different Separation Angles Conditions (aft Joints Disconnection in Different Angles)

In addition to various spring ejector mechanisms, simulation for different separation angles has also been done. In the standard mode (according to figures 22 to 27), spherical joints in the upper section are cut at 0.001 seconds after separation, and consequently, boosters begin to rotate around the aft joints until the boosters reach to 1-degree angle (about z-axis) and aft joints separation. Fig. 22 shows the location of the strap-on boosters at 1.1 seconds after separation with different separation angle conditions. In this figure, the nearest booster to the core refers to standard mode (separation angle is 1-degree) and other two modes refer to 3 degree and 5 degree. Pressure contour variation during strap-on boosters' separation is shown in Fig. 24.

Separation angle conditions that are shown due to delay of the lower joints' disconnection (increasing separation angle), and so aerodynamic forces increase on boosters and separation is improved. This is clearly observed in boosters' center of mass velocity diagrams (velocities are increasing in y-direction) in Fig. 26. As it can be seen in Fig. 23, the spring ejector mechanism is the same for all three cases that are mentioned before. In figures 25, 26, and 27, variations of relative distances of boosters center of mass with time (ΔX, ΔY), relative velocities (ΔVx, ΔVy) and relative accelerations (ΔAx, ΔAy) in presence of aerodynamic effects with different separation angels can be seen.

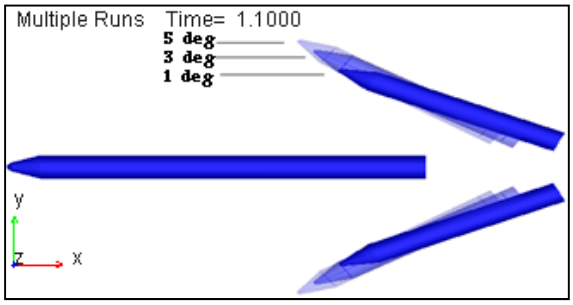

Fig. 22: Boosters' location at t=1.1sec after separation (with various separation angle conditions - using standard ejector springs)

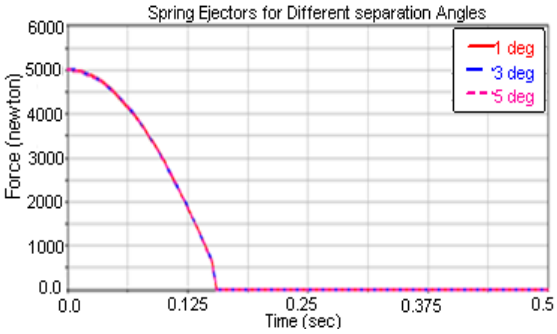

Fig. 23: Time variation of spring1 force for various separation angle conditions

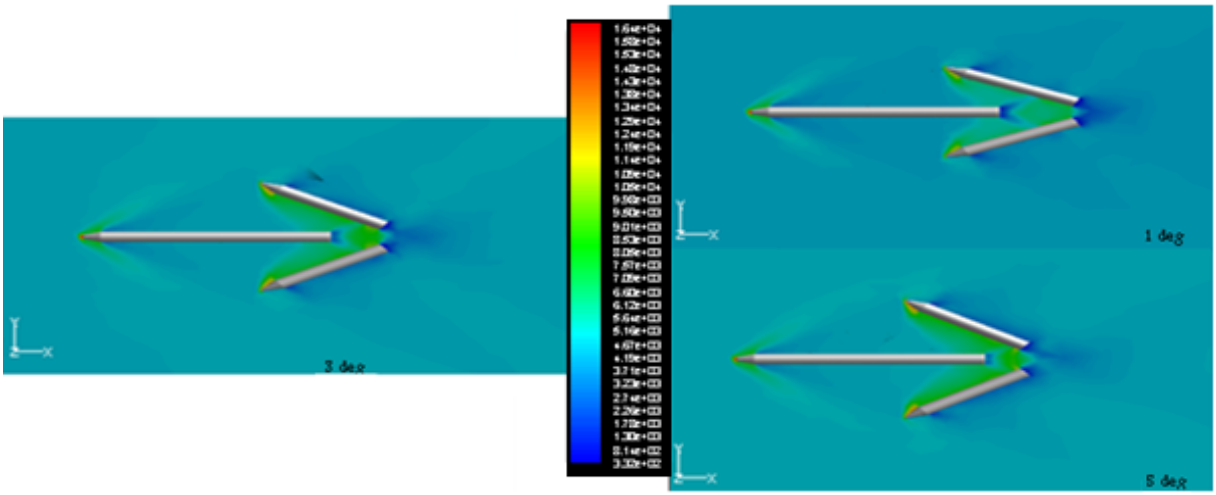

Fig. 24: Pressure contour variation around the launch vehicle and boosters at t=1.1sec after separation (with various separation angle conditions - using standard ejector springs) CM) with time with various separation angle conditions (in the presence of aerodynamic effects)

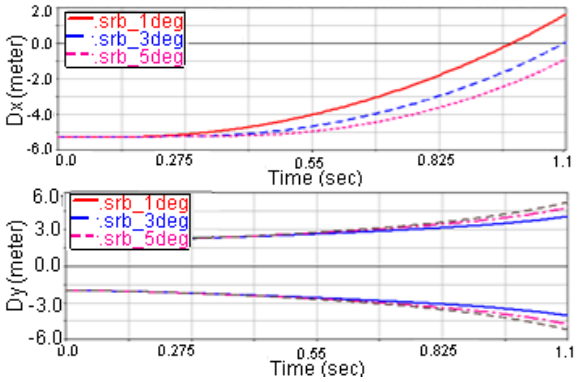

Fig. 25: Variation of strap-on boosters' relative distances, ΔX, ΔY (relative to the core CM) with time with various separation angle conditions (in the presence of aerodynamic effects)

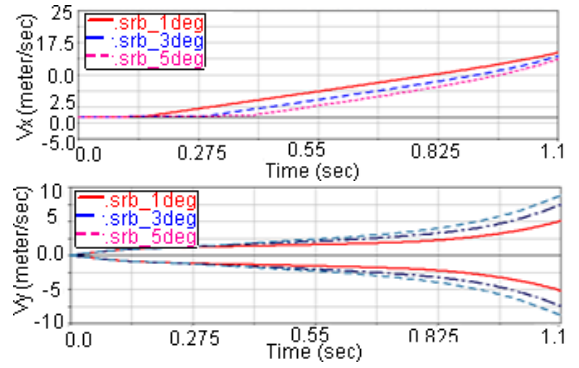

Fig. 26: Variation of the left & right boosters' relative velocities, ΔVx, ΔVy (relative to the core CM) with time with various separation angle conditions (in the presence of aerodynamic effects)

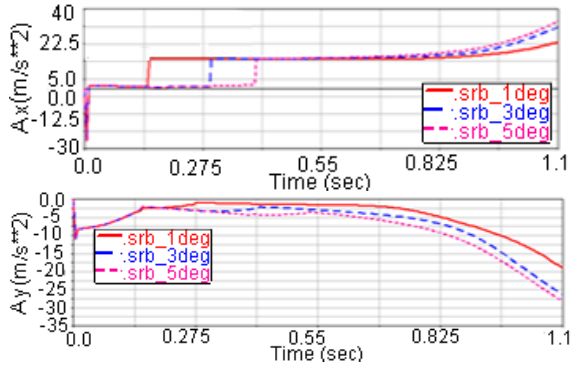

Fig. 27: Variation of the left & right boosters' relative translational accelerations, Ax, Ay (relative to the core

Conclusion

In this study, 6DOF strap-on boosters' separation from the launch vehicle was presented. In addition to spring ejector mechanisms and constraint joints, aerodynamic forces and moments were considered using coupled constraint dynamics and numerical aerodynamics. As mentioned, the strap-on boosters' separation from launch vehicle has already been studied in the literature. However, in all of the previous works, just one of the dynamics' motion or flow aerodynamics was simulated precisely, and the other was modeled simple or prescribed. Separation simulation methods in dense atmosphere can be classified in four summarized groups as can be seen in table 3.

According to table 3, the methods 1, 2, and 3 has already been used for separation simulation in dense atmosphere. For example, the method 3 can be performed in such software like FLUENT [7, 8, and 9], that the dynamics of motion and mechanisms are coupled as a UDF (user defined function) to flow solver. However, in this method, there is no possibility to model the full separation mechanisms (like joints, etc.). In this paper, according to method 4 in table3, the first version of the software code with name of IRASEP for real-time simulation of coupled dynamics and aerodynamics of constrained strap-on boosters from launch vehicle was presented. The ability of this interface software in connection of multi-body dynamics solver and the numerical aerodynamic solver has provided a high potential in separation simulation in the dense atmosphere.

Table 3: comparison of different separation simulation methods in dense atmosphere

	Dynamics	aerodynamics	Description
1	Simulation of separation dynamics with mechanisms modeling	Offline aerodynamic lookup table	High costs for generating multidimensional aerodynamics table-inaccurate aerodynamics []
2	Prescribed motion	Time-dependent aerodynamics (unsteady)	inaccurate dynamics
3	Simulation of separation dynamics with Brief mechanisms modeling (real-time coupled with the aero dynamics)	-Quasi-static aerodynamics -Time-dependent aerodynamics (unsteady)	inaccurate erodynamics (quasi-static) Impossibility of modeling the full separation mechanisms (like joints, etc.)
4	Simulation of separation dynamics with complete mechanisms modeling (real-time coupled with the aerodynamics)	Time-dependent aerodynamics (unsteady)	modeling the full separation mechanisms in presence of Time-dependent aerodynamic effects

In this simulation, two time-dependent solvers of unsteady dynamics and aerodynamics are completely independent of each other and just exchange the information through an interface software. Thus, more accurate modeling of dynamic mechanisms in the presence of unsteady aerodynamics than conventional methods is possible. The accuracy of this numerical simulation was proved by real-time simulation of joints' separation in the presence of unsteady aerodynamics as an example which was not provided in any of the

references so far. Considering the presented diagrams and separation animations, importance of aerodynamics effects in strap-on booster separation simulation in the mentioned conditions is quite evident.

References

[1]. Jafari, M., Toloei, A., Ghasemlu, S., Parhizkar, H." Simulation of Strap-on Boosters Separation in the Atmosphere", International Journal of Engineering (IJE), Transactions B: Applications, Vol. 28, No. 2, (February 2015), pp. 164-171.

[2]. Meakin, R.L., and Suhs, N. E., "Unsteady Aerodynamic Simulation of Multiple Bodies in Relative Motion" AIAA Paper 89-1996, 1989.

[3]. Lochan, R., and Adimurthy, V., "Separation Dynamics of Strap-On Boosters in the Atmosphere," Journal of Guidance, Control, and Dynamics, Vol. 20, No. 4, 1997, pp. 633–639.

[4]. Lijewski, L. E., and Suhs, N. E., "Time-Accurate Computational Fluid Dynamics Approach to Transonic Store Separation Trajectory Prediction," Journal of Aircraft, Vol. 31, No. 4, 1994, pp. 521–526.

[5]. Taylor, S., and Wang, J. C. T., "Launch-Vehicle Simulations Using a Concurrent, Implicit Navier–Stokes Solver," Journal of Spacecraft and Rockets, Vol. 33, No. 5, 1996, pp. 601–606.

[6]. Azevedo, J. L. F., and Moraes, P., Jr., "Code Validation for High-Speed Flow Simulation Over Satellite Launch Vehicle," Journal of Spacecraft and Rockets, Vol. 33, No. 1, 1996, pp. 15–21.

[7]. Seongjin Choi, Chongam Kima, Oh-Hyun Rho, Jeong-joo Park, "Numerical Analysis on Separation Dynamics of Strap-On Boosters in the Atmosphere", Journal of Spacecraft and Rockets, Vol. 39, No. 3, May–June 2002

[8]. Soon-Heum Ko and Chongam Kim, "Separation Motion of Strap-On Boosters with Base Flow and Turbulence Effects", Journal of Spacecraft and Rockets, Vol. 45, No. 3, May–June 2008

[9]. "Transonic store separation using unstructured cfd with dynamic meshing", Technical Report AIAA-2003-3913

[10]. D. O. Snyder, E. K. Koutsavdis, and J. S. R. Anttonen, "Simulations of 6-DOF Motion with a Cartesian Method". Scott M. Murman, ELORET Moffett Field, CA. Michael J. Aftosmis, NASA Ames Research Center, Moffett Field, CA. Marsha J. Berger, Courant Institute, New York, NY. 41st AIAA Aerospace Sciences Meeting, January 6-9, 2003 / Reno, NV.

[11]. D. O. Snyder, E. K. Koutsavdis, and J. S. R. Anttonen, "Transonic store separation using unstructured cfd with dynamic meshing", Technical Report AIAA-2003-3913.

[12]. Bandu N. Pamadi, Nathaniel J. Hotchko, Jamshi Samareh, Peter F. Covell, and Paul V. Tartabini, "Simulation and Analyses of Multi-Body Separation in Launch Vehicle Staging Environment", 14th AIAA/AHI Space Planes and Hypersonic Systems and Technologie Conference AIAA 2006-803.

[13]. Kelly J. Murphy, Pieter G. Buning, Bandu N. Pamadi, William I. Scallion, Kenneth M. Jones, "Overview of Transonic to Hypersonic Stage Separation Tool Development for Multi-Stage-To-Orbit Concepts", NASA Langley Research Center, AIAA 2004-2595.

[14]. Pamadi, B.N., Neirynck, T.A., Covell, P.F., Hotchko, N.J., and Bose, D.M., "Simulation and Analyses of Staging Maneuvers of Next Generation Reusable Launch Vehicles", AIAA Paper 2004-5185.

[15]. Pamadi, B.N., Neirynck, T.A., Hotchko, N.J., Tartabini, P.V., Scallion, W.I., Murphy, K.J., and Covell, P. F., "Simulation and Analyses of Stage Separation of Two-Stage Reusable Launch Vehicles", AIAA Paper 2005-3247.

[16]. Bandu N. Pamadi, Paul V. Tartabini, Mathew D. Toniolo, Carlos M. Roithmayr, Christopher Karlgaard, and Jamshid Samareh, "Application of CFE/POST2 for Simulation of Launch Vehicle Stage Separation", NASA Langley Research Center, Hampton VA 23681.

[17]. Toniolo, M. D., Tartabini, P. V., Pamdai, B. N., and Hotchko, N., "Constraint force equation methodology for modeling multi-body stage separation dynamics", 46th AIAA Aerospace Sciences Meeting & Exhibit, 7-10 January 2008.

[18]. Tartabini, P. V., Roithmayr, C., Toniolo, M. D., Karlgaard, C., and Pamdai, B. N., "Verification of the constraint force equation methodology for modeling multi-body stage separation", AIAA Modeling and Simulation Technologies Conference, 18-21 August 2008.

[19]. Jafari, M., Toloei, A., Ghasemlu, S., Parhizkar, H. "Simulation of Store Separation using Low-Cost CFD with Dynamic Meshing", International Journal of Engineering Transactions B: Applications, Vol. 27, No. 5, May 2014, pp. 853-863.

[20]. Jafari, M., Toloei, A., Ghasemlu, S., Parhizkar, H. "6dof Simulation of Store Separation using CFD", The 11th conference of Iranian Aerospace society, March 2012, Tehran, Iran.

[21]. Dalle, D. J., Rogers, S. E., Lee, H. C., Chan, W. M., "Inviscid and Viscous CFD Analysis of Booster Separation for the Space Launch System Vehicle", 54th AIAA Aerospace Sciences Meeting. January 2016, 10.2514/6.2016-0797.

[22]. Rogers, S. E., Dalle, D. J., Chan, W. M., CFD Simulations of the Space Launch System Ascent Aerodynamics and Booster Separation, AIAA Paper 2015-0778, 53rd AIAA Aerospace Sciences Meeting, January, 2015.